Received: 10 June 2022 | Revised: 13 July 2022 | Accepted: 19 July 2022

DOI: 10.1111/jon.13031

JOURNAL OF NEUROIMAGING
THE OFFICIAL JOURNAL OF THE AMERICAN SOCIETY OF NEUROIMAGING
WILEY

REVIEW ARTICLE

Brain topography on adult ultrasound images: Techniques, interpretation, and image library

Sahil Kapoor[1] | Austin Offnick[2] | Beddome Allen[3] | Patrick A. Brown[4] | Jeffrey R. Sachs[5] | Metin Nafi Gurcan[6] | Gianmarco Pinton[7] | Ralph D'Agostino Jr[8] | Cheryl Bushnell[9] | Stacey Wolfe[10] | Pam Duncan[9] | Andrew Asimos[11,12] | Aarti Sarwal[9]

[1]Department of Neurology, Wake Forest Baptist Medical Center, Winston-Salem, North Carolina, USA

[2]Department of Neurology, Wake Forest Baptist Medical Center, Winston-Salem, North Carolina, USA

[3]Department of Neurology, Wake Forest School of Medicine, Winston-Salem, NC, USA

[4]Departments of Radiology and Neurosurgery, Wake Forest School of Medicine, Winston-Salem, North Carolina, USA

[5]Neuroradiology Section, Wake Forest School of Medicine, Winston-Salem, North Carolina, USA

[6]Center for Biomedical Informatics, Wake Forest School of Medicine, Winston-Salem, North Carolina, USA

[7]Joint Department of Biomedical Engineering, University of North Carolina at Chapel Hill & North Carolina State University, Chapel Hill, North Carolina, USA

[8]Department of Biostatistics and Data Science, Wake Forest School of Medicine, Winston-Salem, North Carolina, USA

[9]Department of Neurology, Wake Forest School of Medicine, Winston-Salem, North Carolina, USA

[10]Department of Neurosurgery, Wake Forest School of Medicine, Winston-Salem, North Carolina, USA

[11]Department of Emergency Medicine, Wake Forest School of Medicine, Winston-Salem, North Carolina, USA

[12]Carolinas Stroke Network, Atrium Health, Charlotte, North Carolina, USA

Correspondence
Sahil Kapoor, Department of Neurology, Wake Forest Baptist Medical Center, 1 Medical Center Blvd, Winston-Salem, NC 27157, USA.
Email: skapoor@wakehealth.edu

Funding information
Neuroscience Clinical Trials and Innovations Center (NCTIC), Wake Forest School of Medicine

Abstract

Background and Purpose: Many studies have explored the possibility of using cranial ultrasound for discerning intracranial pathologies like tumors, hemorrhagic stroke, or subdural hemorrhage in clinical scenarios where computer tomography may not be accessible or feasible. The visualization of intracranial anatomy on B-mode ultrasound is challenging due to the presence of the skull that limits insonation to a few segments on the temporal bone that are thin enough to allow transcranial transmission of sound. Several artifacts are produced by hyperechoic signals inherent in brain and skull anatomy when images are created using temporal windows.

Methods: While the literature has investigated the accuracy of diagnosis of intracranial pathology with ultrasound, we lack a reference source for images acquired on cranial topography on B-mode ultrasound to illustrate the appearance of normal and abnormal structures of the brain and skull. Two investigators underwent hands-on training in Cranial point-of-care ultrasound (c-POCUS) and acquired multiple images from each patient to obtain the most in-depth images of brain to investigate all visible anatomical structures and pathology within 24 hours of any CT/MRI imaging done.

Results: Most reproducible structures visible on c-POCUS included bony parts and parenchymal structures. Transcranial and abdominal presets were equivalent in elucidating anatomical structures. Brain pathology like parenchymal hemorrhage, cerebral edema, and hydrocephalus were also visualized.

Conclusions: We present an illustrated anatomical atlas of cranial ultrasound B-mode images acquired in various pathologies in a critical care environment and compare our findings with published literature by performing a scoping review of literature on the subject.

KEYWORDS
brain echography, cranial ultrasound, neuro-ultrasound, ultrasonography

INTRODUCTION

During the past several decades, CT and MRI have become the most common modalities for detection of intracranial pathology. With emerging applications of point-of-care ultrasound in emergency medicine and critical care, there has been an increasing interest in exploring the use of cranial ultrasound in the evaluation of patients with suspected brain injury in situations in which CT/MRI is either not available or not feasible due to clinical reasons, such as patient instability. There have been investigations into the use of cranial ultrasound in diagnosis of intracranial hemorrhage, subdural hemorrhage, hydrocephalus, tumors, and movement disorders, but there is currently no standard reference to describe the normal or abnormal B-mode sonographic appearance of the structures of the brain and skull. Our study explores the topography of the brain on B-mode ultrasound in adult critically ill patients and provides descriptive examples of the anatomical and pathological structures that can be visualized on B-mode cranial ultrasonography. We hope the results of this study provide a pictorial reference library of sonographic cranial topography to serve further investigations in cranial ultrasound applications.

METHODS

Study design

After obtaining approval from Institutional Review Board IRB00048743, we screened patients admitted to the neurocritical care unit from October 1, 2021 to May 12, 2022, the period when research study enrollment was allowed by institutional guidelines (Figure 1). Adult patients ≥18 years of age were prospectively enrolled if they were able to receive a cranial ultrasound scan within 24 hours of cross-sectional cranial imaging (CT or MRI) performed as part of routine evaluation and care for assessment of intracranial pathology. Our previous exploratory study in 11 patients performed in 2020 formed the basis of this study.[1] Two investigators (AO and SK) were trained in cranial ultrasound by a senior investigator (AS) by a didactic review of intracranial anatomy and pathology. Hands-on scanning of three healthy volunteers (AS, AO, and SK) to learn ultrasound-based cranial anatomy and ultrasound acquisition technique was followed by five supervised cranial ultrasound scans on critically ill patients performed after reviewing patient's CT/MRI images. Cranial ultrasound images were then obtained by trained investigators (AO and SK) blinded to patients' CT scans and archived in QPath™ E (Telexy). Patients were excluded from the study if the patient, bedside family, or nursing staff declined an ultrasound scan, the patient had any penetrating head trauma or skull defects that could affect ultrasound insonation,[2] and if images could not be obtained within 24 hours of last or expected CT or MRI imaging to ensure corresponding acute pathology was imaged. Patients being evaluated for coronavirus disease 2019 (COVID-19) or in contact precautions due to confirmed COVID-19 were also excluded. Consent was obtained from the patient or their legally authorized representative, in person or via DocuSign®. Investigators also aborted scans if they perceived subjective patient discomfort or agitation after initiation of the scan. The study recruitment period and consents reflect the impact of pandemic-imposed research enrollment restrictions.

Ultrasound imaging acquisition

Point-of-care ultrasound machines (Fujifilm, SonoSite® Xporte) available in the patient care unit utilizing a low-frequency 3-1 MHz phased array probe (echo probe) were used to acquire B-mode images of the brain via the temporal window on the transcranial and abdominal presets. A point-of-care device was chosen for the study to reflect the typical clinical scenarios for use of cranial ultrasound in which traditional cross-sectional neuroimaging or advanced ultrasound machinery is not available. Scans were conducted at the bedside with the patient in supine positioning, with the head of the bed at 30 degrees from horizontal. During scanning, the probe is positioned on the temple to align the line of insonation with an imaginary line from

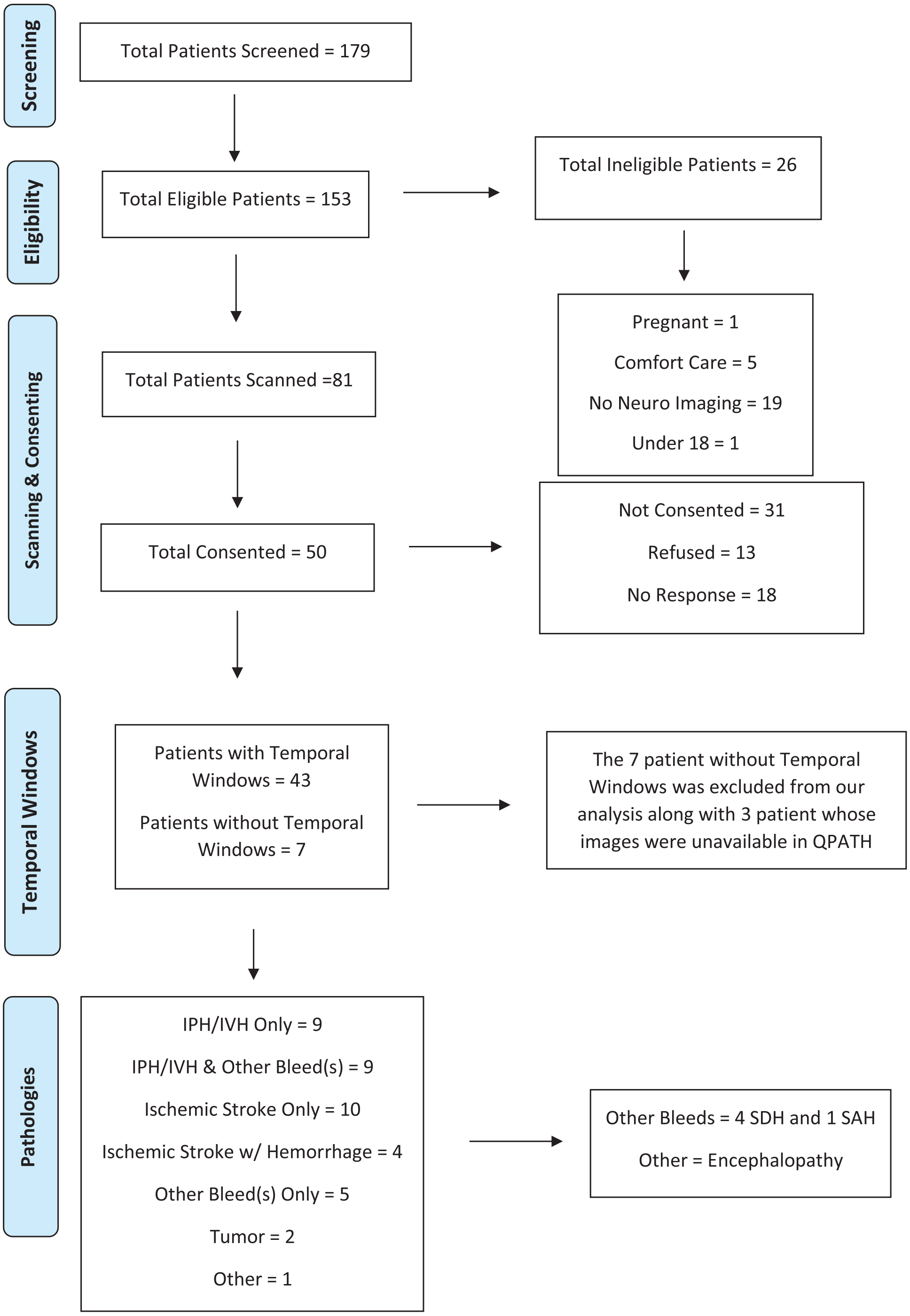

FIGURE 1 CUPIDICU flow diagram displaying the enrollment process. Screened patients from October 1, 2022 to May 12, 2022; paused enrollment between October 7, 2022 and October 18, 2022; November 28, 2021 and January 1, 2022; and March 15, 2022 and May 2, 2022, to work through consents, conduct data analysis, and review images (CUPIDICU, cranial ultrasound for point of care intracranial hemorrhage detection in patients in the intensive care unit; IVH, Intraventricular hemorrhage; IPH, intraparenchymal hemorrhage; SDH, subdural hemorrhage; SAH, subarachnoid hemorrhage).

the lateral canthus of the eye to the tragus of the ear with index marker pointed anteriorly. Image depth is adjusted until the opposite skull is visualized. Once the skull is visualized, reflecting the presence of temporal windows, the probe direction is then adjusted to visualize the butterfly-shaped midbrain, allowing distinction of ipsilateral and contralateral cerebral hemispheres. The probe is then directed further anteriorly, posteriorly, superiorly, and inferiorly. Images depicting discernible intracranial anatomy were captured on the transcranial and abdominal preset on both sides of the brain. Any structures visible as white or bright in comparison to the skull were labeled as "hyperechoic" and any structure visible as gray or black compared to the skull was labeled as "hypoechoic." The total duration of each scan was 5-20 minutes to image both the right- and left-side windows under both presets.

Image analysis

All images acquired were compared post hoc with CT/MRI results to elucidate cranial anatomy and pathology by study investigators (AO, SK) and senior study investigators with training in neurocritical care and neurosonology (AS) and neuroradiology (PB, JS) to corroborate cranial topography.

Literature review

Independent investigators (BA, SK) performed a scoping review of published literature according to Preferred Reporting Items for Systematic Reviews and Meta Analysis guidelines on electronic databases PubMed, Cochrane, Embase, Scopus, Web of Science, and Cumulative Index to Nursing and Allied Health Literature for English language studies published between January 1990 and July 2021 comparing B-mode transcranial ultrasound with conventional imaging (CT/MRI) in adults or children. Studies were interrogated for medical subject headings (MeSH) terms: ultrasound, Doppler, transcranial, brain ultrasound, ultrasonography, and cranial ultrasound. Neonatal transfontanelle sonographic studies were excluded. Eligible publications were reviewed for the description of any intracranial structures, and representative images were retrieved. Study images were then compared to images available in published literature.

RESULTS

Image analysis

During the enrollment period, 179 patients were screened, and 50 consented to participate. Of these, 7 patients had no temporal windows (Figure 1). Patients tolerated the imaging well in our study, and less than 5% of scans had to be aborted due to patient discomfort or agitation. The most common reasons for ineligibility were inability to obtain consent, lack of temporal windows, and overlying materials (eg, head wraps, electroencephalogram leads, and surgical drains) precluding sonographic imaging.

Several artifacts were visualized that created hyperechoic signals corresponding to known structures in brain and skull anatomy described below. Anatomical landmarks, in general, were better identifiable on cine loops during dynamic imaging rather than saved snapshots of B-mode images. Both the transcranial and abdominal preset were equivalent in elucidating anatomical structures. Disabling tissue harmonic imaging on abdominal presets allowed for better visualization of anatomical structures. Contralateral cerebral hemispheric structures were better visualized on B-mode ultrasound imaging due to obscuration of ipsilateral structures related to artifacts produced by the ipsilateral sphenoid wing.

Literature review

A total of 290 articles that described the selected MeSH terms were identified in our literature review. After a detailed review, we selected 44 articles that described any intracranial pathology in comparison to CT or MRI using B-mode ultrasound (Figure 2).

Topography of normal anatomical structures on cranial ultrasound imaging

Below is an outline of the most discernible anatomical structures visible on B-mode imaging in patients with temporal windows and the comparison with anatomical structures described in indexed literature.

Bony landmarks of the skull

The presence of temporal windows was discernible by the visualization of opposite skull seen as a hyperechoic convex structure in most patients (Figure 3). Many other anatomical structures were easily visible in patients as hyperechoic signals similar to the opposite skull and are described below. We did not find any specific mention of bony landmarks described in the literature upon our systematic review.

a. Opposite skull: a hyperechoic convex structure corresponding to the curve of the skull. This landmark is used to confirm the presence of temporal windows (Figures 3 and 5; Video S1)
b. Frontal bone: visualized by moving the probe anteriorly after confirming the presence of temporal windows (Figure 4; Video S1)
c. Occipital bone: hyperechoic structure—visualized by moving the probe posteriorly toward patient's occiput (Figure 5; Video S2)
d. Ipsilateral convex ridge: hyperechoic artifact produced by lesser wing of the sphenoid and petrous part of the temporal bone ipsilateral to the temporal windows closest to the probe (Figure 3; Videos S3 and S5). This landmark defines the ipsilateral middle cranial fossa.
e. Contralateral convex ridge: hyperechoic artifact created by lesser wing of the sphenoid and petrous part of the temporal bone contralateral to the temporal windows (Figures 3 and 6; Videos S3 and S5). This landmark defines the contralateral middle cranial fossa.
f. Clivus with anterior clinoid processes visible as two hyperechoic spots on either side of the midline near the midbrain (Figure 3; Video S3).
g. Orbital fossa: visible inferiorly near frontal bones as a round structure on either side of the midline (Figure 7).
h. Ridge in the occipital bone that marks the location of the transverse venous sinus (Figure 8).

Intracranial Pathology Scoping Review: Table

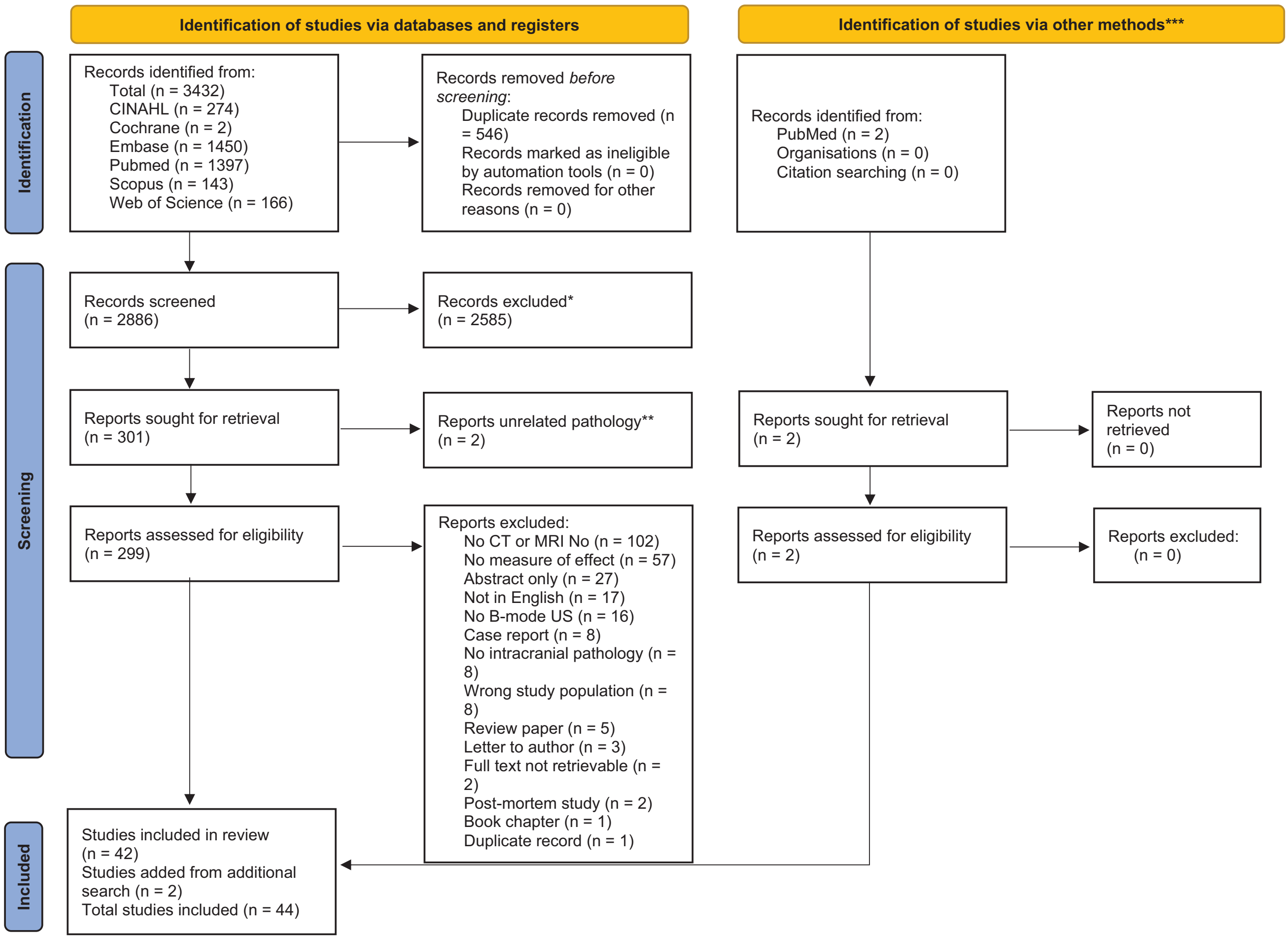

Inclusion criteria	Exclusion criteria
1. Studies published between January 1990 and July 2021. 2. Study designs include randomized controlled trials, comparative cohort studies, case-control studies, case series with > 3 patients, and cross-sectional studies. 3. Imaging methods including B mode cranial ultrasound through the temporal window in addition to MRI, CT, single-photon emission computed tomography (SPECT), or positron emission tomography (PET) of the head. 4. Subjects with intracranial, parenchymal, nonvascular pathology confirmed by MRI, CT, SPECT, or PET of the head. 5. Study subjects including children, adolescents, or adults without fontanelle ultrasound windows.	1. Case reports and case series with < 4 patients, review papers, studies not written in English, study populations including neonates with fontanelle windows, postmortem studies, transfontantelle disorders, germinal matrix hemorrhages, skull disorders, and grey literature (non-peer reviewed e.g., conference abstracts and book chapters). 2. Studies were additionally excluded if only Doppler studies were performed, if a gold standard imaging was not performed, or if transcranial B mode ultrasound was not performed. 3. Studies that did not report a measure of effect were excluded.

FIGURE 2 PRISMA (Preferred Reporting Items for Systematic Reviews and Meta Analysis) diagram demonstrating the study selection process (*n*, number of studies; CINAHL, Cumulative Index to Nursing and Allied Health Literature; US, ultrasound)

Brain

Brain parenchymal details in general were not distinguishable and appeared as a hypoechoic signal without much distinction between sulci and gyri, white or gray matter. The following structures were reproducibly discernible on B-mode imaging in our study:

a. Midbrain: easily visible structure located in the center of the cranium in the shape of a butterfly with wings representing the peduncles (Figures 3, 6, and 9; Video S3). We found 15 publications that describe midbrain or brainstem landmarks.[3–19]
b. Basal cisterns: hyperechoic signals in cisterns around the midbrain with signal intensity lower than bone when compared to opposite skull[19,20] (Figures 3 and 9).
c. Falx cerebri: hyperechoic line in the middle of the cranium toward the frontal bone with probe pointed superiorly[9] (Figures 4, 5, and 9).
d. Thalami: visible as two bean-like structures on moving the probe superior to the midbrain[7,17,21,22] (Figures 5 and 12; Video S6).
e. Cerebral aqueduct: a dot-like hyperechoic structure within the posterior end of the midbrain (Figures 9 and 10).

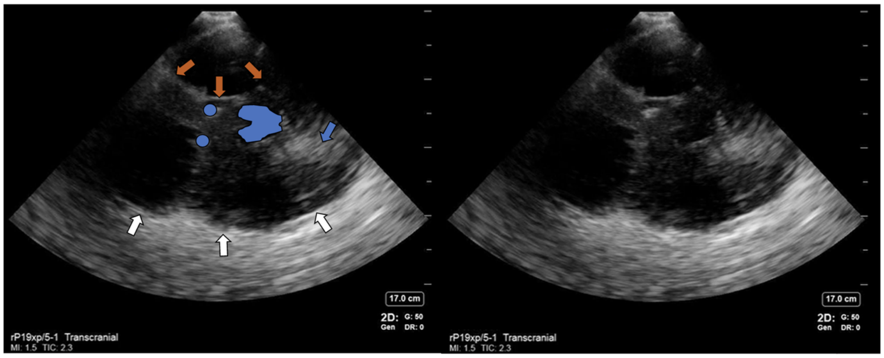

FIGURE 3 Cranial ultrasound image showing opposite skull (white arrows), ipsilateral convex ridge produced by lesser wing of the sphenoid bone and petrous part of the temporal bone (orange arrows), midbrain (butterfly-shaped blue structure), and clinoid processes (blue dots). Contralateral brain parenchyma is better visualized compared to ipsilateral parenchyma. Trailing bright signal below the midbrain with hyperechoic signals resembling signals produced by a hemorrhage (blue arrow)

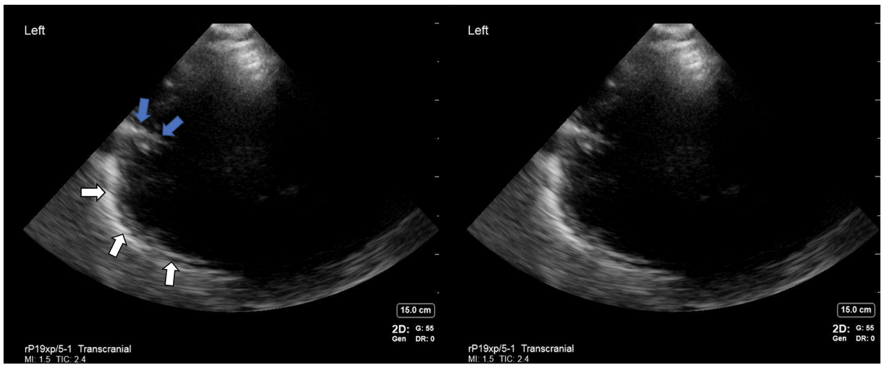

FIGURE 4 Cranial ultrasound image showing opposite skull frontal bone (white arrows) and falx cerebri (blue arrows) in areas of frontal bone as hyperechoic structure

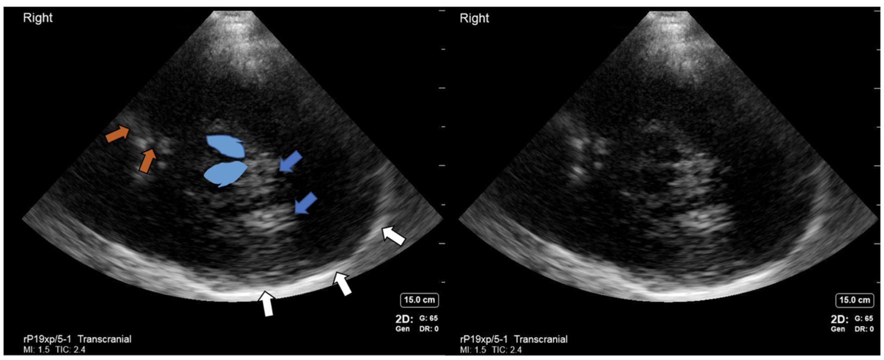

FIGURE 5 Cranial ultrasound image showing opposite skull (white arrows) and falx cerebri (orange arrows) in area of occipital bone as hyperechoic structure. The center of the cranium shows two bean-shaped structures (blue) corresponding to the thalami. Trailing bright signal below the midbrain with hyperechoic signal resembling signals produced by a hemorrhage (blue arrows)

f. Calcified choroid plexus: visible as three spaced hyperechoic signals with the appearance of "a spaceship" in the middle of the cranium[9] (Figure 11; Video S2).
g. Lateral ventricles: two anechoic structures visible in the temporal or frontal lobes surrounded by hyperechoic margins.[14,17,21,23–26] One publication described measuring the diameter of lateral ventricle in the coronal planes[27] (Figure 11; Video S2).
h. Third ventricle: often visible as two parallel lines sometimes pulsating in the vicinity of midbrain with probe pointed superiorly and anteriorly (Figure 12; Video S6). Eight other publications have described the appearance of third ventricle on cranial ultrasound as an anechoic area surrounded by two hyperechoic margins observed by tilting the probe 10° up after identification of midbrain.[3,7,9,10,14,17,21,28]

JOURNAL OF NEUROIMAGING
THE OFFICIAL JOURNAL OF THE AMERICAN SOCIETY OF NEUROIMAGING
WILEY

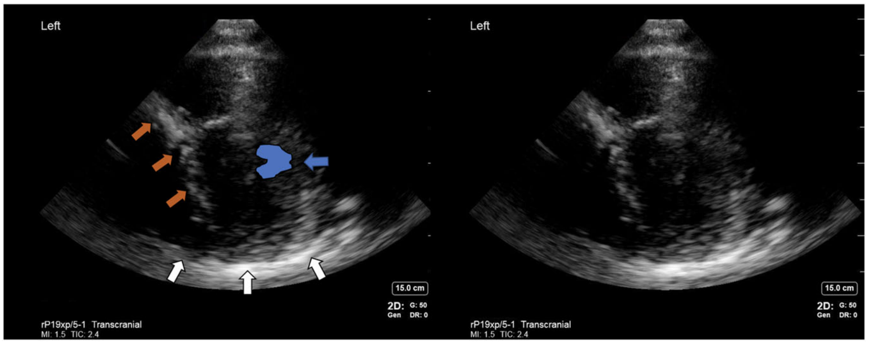

FIGURE 6 Cranial ultrasound image showing contralateral convex ridge produced by the greater wing of the sphenoid bone and petrous part of the temporal bone (orange arrows), midbrain (butterfly-shaped structure) (blue arrow), and opposite skull (white arrows)

FIGURE 7 Cranial ultrasound image showing orbital fossa cavity (blue arrows)

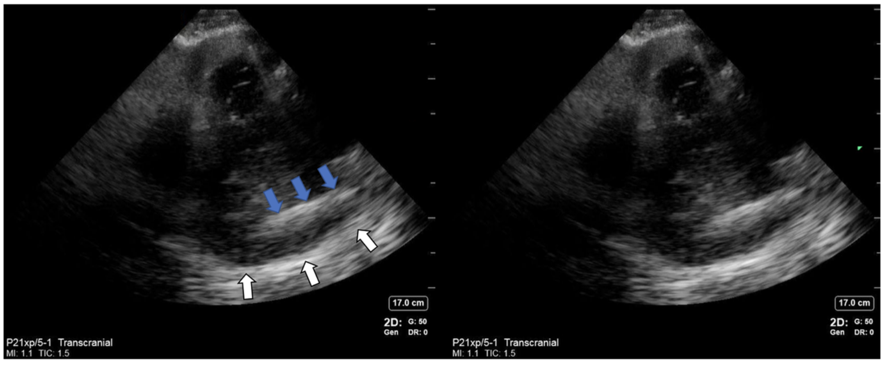

FIGURE 8 Cranial ultrasound showing opposite skull (white arrows) and ridge (blue arrows) in the occipital bone marking the transverse venous sinus location

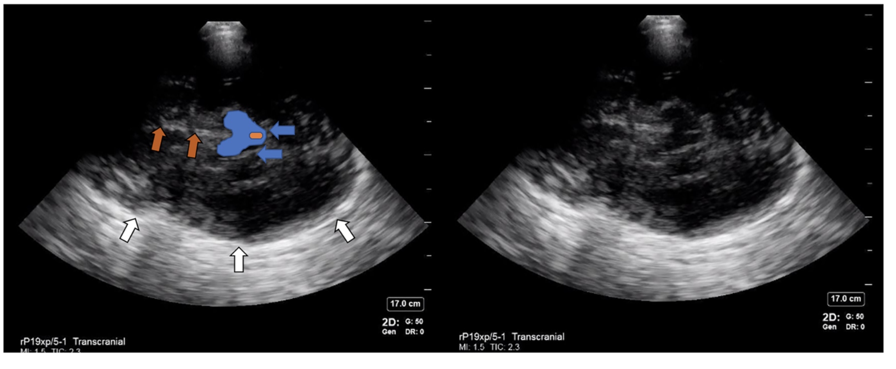

FIGURE 9 Cranial ultrasound image showing falx cerebri (orange arrows), opposite skull (white arrows) with midbrain (blue butterfly-shaped structure), and cerebral aqueduct (orange dot). Contralateral brain parenchyma is better visualized compared to ipsilateral parenchyma. Basal cisterns: Ambient and quadrigeminal cisterns demonstrate hyperechoic signals relative to the adjacent midbrain (blue arrows).

FIGURE 10 B-mode cranial ultrasound image showing no distinguishing features of ischemic stroke with normal appearance of architecture of the brain with attached CT showing changes consistent with ischemia. The opposite skull (white arrows) with midbrain (blue butterfly-shaped structure) and cerebral aqueduct (orange dot) can be visualized.

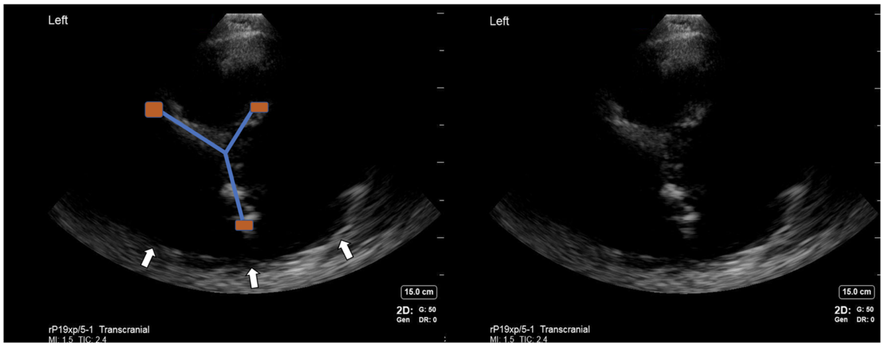

FIGURE 11 Cranial ultrasound image showing lateral ventricles as Y-shaped structure with choroid plexus visible (three orange square dots) with the opposite skull (white arrows)

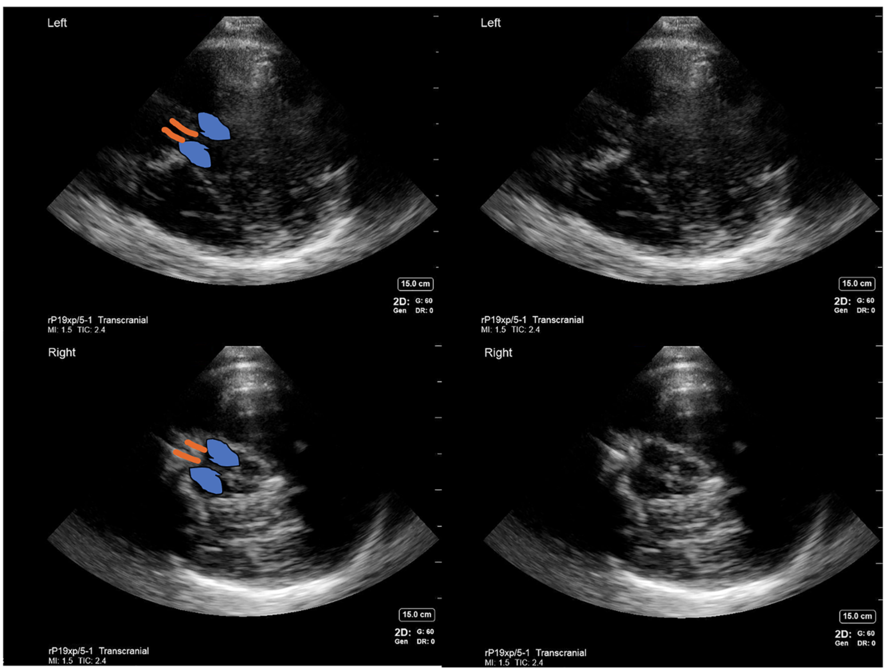

FIGURE 12 Cranial ultrasound displaying normal appearance of third ventricle (orange lines) and bean-shaped structures (blue) corresponding to the thalami

JOURNAL OF NEUROIMAGING THE OFFICIAL JOURNAL OF THE AMERICAN SOCIETY OF NEUROIMAGING WILEY

FIGURE 13 Cranial ultrasound image showing hyperechoic pineal gland (blue arrow) but no distinct appearance of encephalomalacia when compared with the corresponding CT head

i. Pineal gland: a small dot-like structure in the center of the brain posterior to the midbrain. It is described as an echogenic structure in the dorsal part of the third ventricle. Both publications compared pineal glands in normal volunteers with pineal gland cysts in patients[9,10] (Figure 13).
j. Basal ganglia: deep brain structures such as internal capsule, lentiform nucleus, and caudate nucleus were in general not distinguishable on B-mode ultrasound using point-of-care devices. Twenty-one publications have described visualization of substantia nigra[3,4,7,8,11–13,17,19–22,24,28–35]; six manuscripts have described basal ganglia visualization.[3,12,14,16,17,20]

Artifacts

In addition to the above anatomical landmarks, the following reproducible hyperechoic artifacts were identified in multiple scans. This is important to recognize due to their appearance as possible intracranial hemorrhage mimics:

a. Hyperechoic shadows between the midbrain and opposite skull in line of insonation (midbrain acoustic shadow): these may mimic hyperechoic signals produced by a hemorrhage (Figures 3 and 5).
b. Hyperechoic signals parallel to the occipital bone caused by thick skull ridges in the posterior fossa: these may mimic hyperechoic signals produced by a hemorrhage (Figure 8).

Topography of abnormal or pathological structures on cranial ultrasound imaging

Below is an outline of the most discernible pathological structures visible on B-mode imaging in patients with temporal windows and the comparison with intracranial pathology described in indexed literature.

a. Ischemic stroke: not discernible and could not be distinguished distinctly from the rest of the brain parenchyma. We could not discern encephalomalacia on ultrasound, either (Figures 10 and 13). Published literature described the appearance of ischemic stroke similar to normal brain parenchyma with detection of reversal of blood flow using Doppler superimposed with B-mode imaging. No description of encephalomalacia on ultrasound was found in our review.[18,25,27,36]
b. Intracerebral/parenchymal hemorrhage: visualized as a hyperechoic signal reproducible in multiple planes by rocking the probe in anteroposterior and cranial-caudal directions at a location where no other anatomical hyperechoic signal was expected (Figure 14; Video S4). Upper brainstem and supratentorial hemorrhage could be visualized. Lower brainstem and cerebellar hemorrhage could not be visualized by ultrasound. Petechial hemorrhages in general could not be discerned with certainty. Calcifications were discernible from hemorrhage by their echogenicity matching bone more closely with silver crisp white appearance (Figure 14). A total of 15 publications have described the visualization of intracerebral hemorrhage.[23,25,26,36–48]
c. Intraventricular hemorrhage: visualized as a hyperechoic signal in the expected third ventricular location. The appearance of the choroid plexus in the lateral ventricles, in general, created an appearance that could mimic the appearance of hemorrhage but the symmetrical nature of the choroid plexus on each side of the midline with a shape resembling "spaceship" helped distinguish the two (Figure 15). We found no references describing intraventricular hemorrhage in the adult brain and pediatric cases with intact skulls.
d. Subarachnoid hemorrhage (SAH) and intracranial aneurysms could not be visualized for identification on cranial ultrasounds in our study, although 3 patients scanned in our study have coiled or clipped aneurysms. Only one published study showed visualization of SAH with ultrasound.[27]
e. Subdural hematoma: described as hypoechoic fluid collection surrounding the brain parenchyma within skull margins was not well appreciated in our study despite 4 patients scanned in our study having subdural hematoma on corresponding CT scans[38,49,50] (Figure 16).
f. Epidural hematoma: hypoechoic fluid collection surrounding the brain parenchyma has been described in one published study.[38,51] We did not have any patients with epidural hematoma in our enrolled study population.

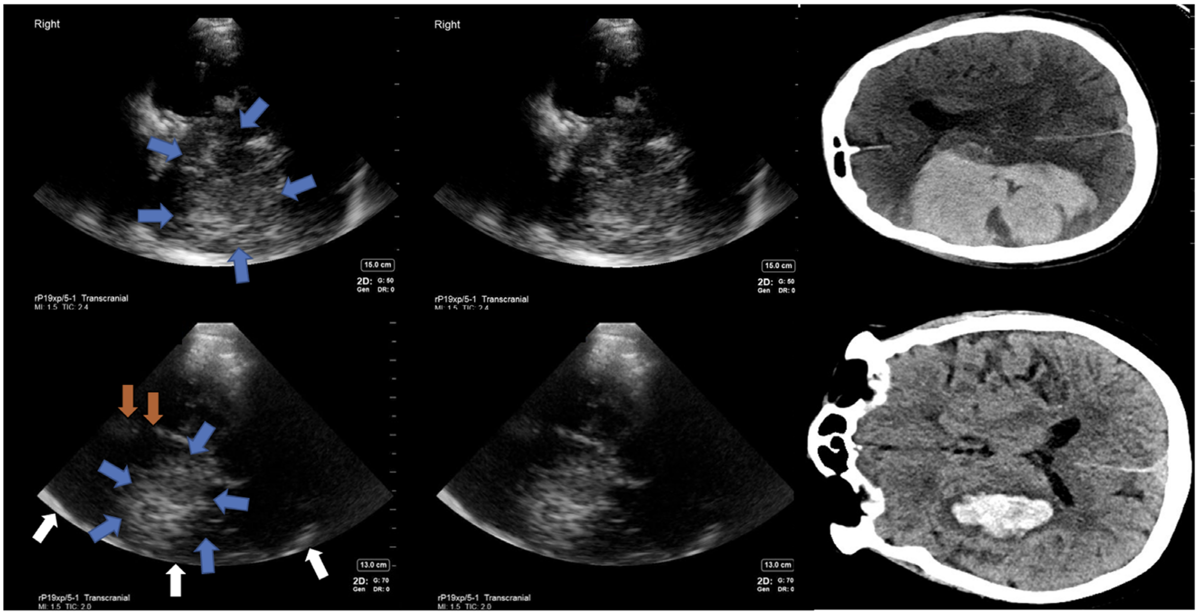

FIGURE 14 Cranial ultrasound image showing intracerebral hemorrhage as region of increased echogenicity (blue arrows), opposite skull (white arrows), and falx cerebri (orange arrows) with the corresponding CT for comparison

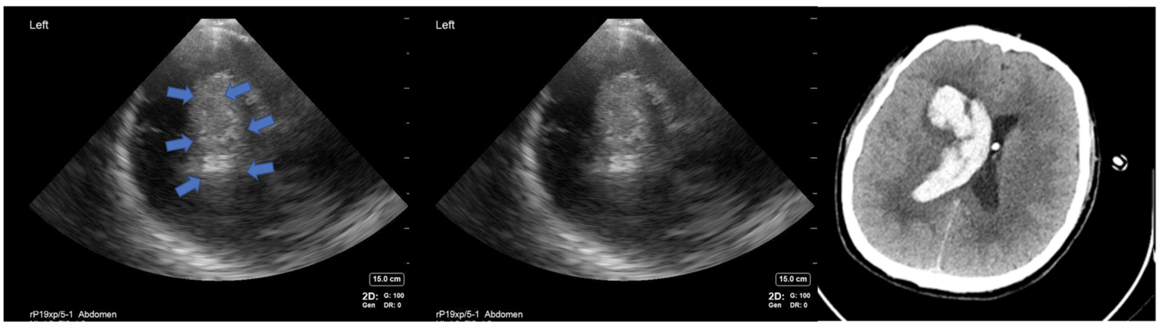

FIGURE 15 Cranial ultrasound image showing intraventricular hemorrhage with intracerebral hemorrhage as region of increased echogenicity (blue arrows) with the corresponding CT for comparison

g. Tumors: visualized as well-defined round structures indistinguishable from hemorrhage. They are described as hyperechoic lesions with an inhomogeneous echotexture depending on the nature of the tumor (Figure 17).[44,52–55]
h. Hydrocephalus: visible as widened third ventricular margins on cranial ultrasound. We were able to visualize enlarged third and lateral ventricles on 1 patient but overall experienced low sensitivity in capturing hydrocephalus, especially involving the lateral ventricles (Figure 18).[27,44]
i. White matter disease and cerebral edema were variably visible as hyperechoic signals and did not have identifying characteristics distinguishing the two. We found five publications that described cerebral edema. We found only one study that showed a sensitivity of diagnosing cerebral edema as visualized by an inability to distinguish diencephalic structures.[27] Other four studies showed a lack of ability to diagnose distinguishing features of cerebral edema by cranial ultrasound.[25,36,37,46]
j. External ventricular drainage catheter-related signals visualized as two parallel lines distinct in their appearance as nonphysiological structures.[56]
k. Pneumocephalus: we could not visualize any distinct characteristics on B-mode ultrasound that allowed the distinction of pneumocephalus from the rest of the cranial structures.

DISCUSSION

The visualization of intracranial anatomy on B-mode ultrasound is challenging due to the presence of the skull, but thin parts of the temporal bone allow transcranial insonation of the brain in a majority

JOURNAL OF NEUROIMAGING
THE OFFICIAL JOURNAL OF THE AMERICAN SOCIETY OF NEUROIMAGING
WILEY

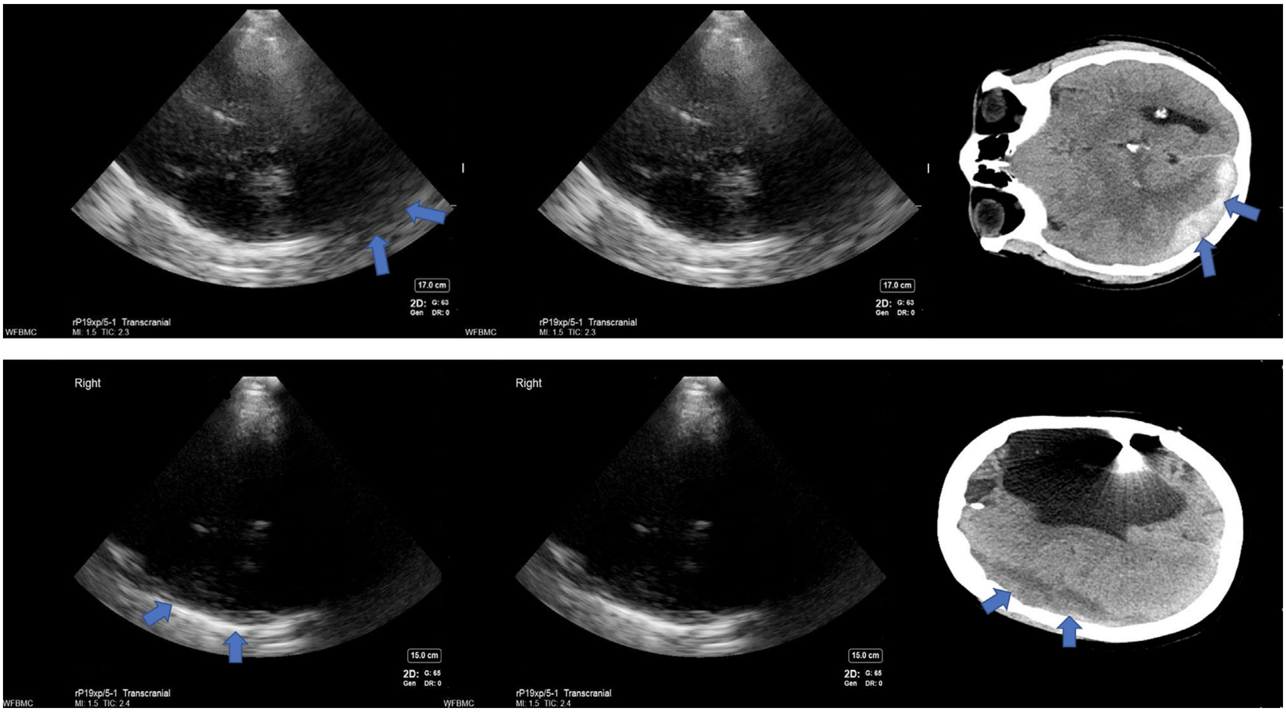

FIGURE 16 Cranial ultrasound image showing indistinct appearance of mixed-density subdural hygroma and hemorrhage (blue arrows) compared with the corresponding CT head

FIGURE 17 Cranial ultrasound displaying thalamic tumor (blue arrows) that has similar appearance to hemorrhagic stroke (false positive) with corresponding CT for comparison

of patients. For patients who do not have temporal windows, several anatomical and pathological structures are distinguishable by their specific appearance in relation to shape, boundary, and anatomical locations. Various abnormal pathologies are also discernable by their echogenicity and abnormal locations.

Multiple prior studies have compared the sensitivity of cranial ultrasound in assessing hemorrhage,[23,25,26,36–48] stroke,[25] or tumor.[44,52–55] However, there is no standard reference resource for cranial topography to outline the appearance of normal and abnormal structures of the brain on B-mode imaging. We provide a descriptive review of the topography of the normal and abnormal brain with illustrative images of different structures visible on B-mode cranial ultrasound in the critically ill population. We also provide comparative references in published literature describing normal and abnormal structures in the brain across a wide range of emergency pathologies. This pictorial library of ultrasound-based anatomy and pathology with the corresponding CT images can guide the design of future studies to assess the accuracy of cranial ultrasound.

Despite our intention to create an exhaustive resource for cranial ultrasound images, we recognize several limitations in our study, most notably small sample size. We did not capture the natural history of intracranial pathology by comparing serial scans for each diagnosis. Acute intracranial pathologies such as cerebral abscess, cerebritis, metabolic encephalopathies, and posterior reversible encephalopathy syndrome, among others, were not able to be captured since serial neuroimaging is not common in these scenarios in the acute period.

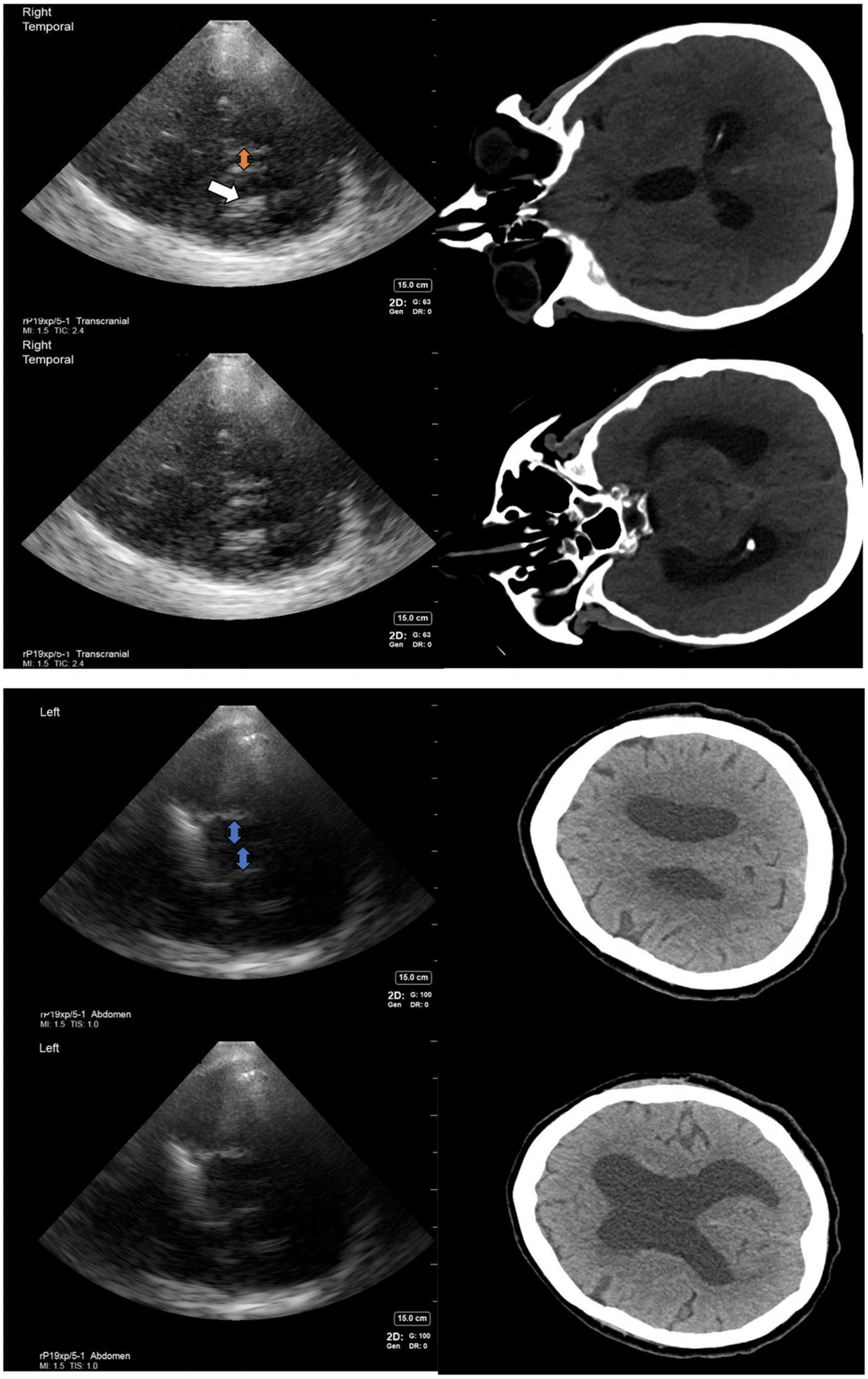

FIGURE 18 Cranial ultrasound image showing enlarged lateral ventricles in a patient with hydrocephalus with corresponding CT head. Dilated third ventricle (orange arrow) and choroid plexus visible inside the temporal horn of lateral ventricle (white arrow) can be seen. Dilated lateral ventricles (blue arrows) can be seen close to the vertex.

For each diagnosis, a full range of pathological variety in terms of size, location, and types was not captured due to limited sample size. Our study is limited by restriction to critically ill population and the use of point-of-care ultrasound devices, which typically may result in lower resolution images. The use of advanced diagnostic machines may render higher resolution images and elucidate more structures with better anatomical detail. Since the settings of most point-of-care applications of cranial ultrasound are likely to be neuro-emergencies not amenable to CT and MRI due to patient location or clinical condition, we felt the use of point-of-care machines appropriate to represent the topography and description of what could be visualized by similar machines available in such scenarios.

JOURNAL OF NEUROIMAGING THE OFFICIAL JOURNAL OF THE AMERICAN SOCIETY OF NEUROIMAGING WILEY

Despite the limitations of insonation restricted to temporal windows, low image resolution with point-of-care devices, and difficulties inherent to critically ill population, cranial ultrasound can be a useful neuroimaging adjunct when temporal windows are present and traditional CT or MRI imaging is inaccessible. This image library can be a useful reference for future studies investigating the utility of cranial ultrasound in various clinical applications.

ACKNOWLEDGEMENTS AND DISCLOSURES

The study team acknowledges the support of institutional review board and other regulatory committees in adapting to the challenges imposed by the pandemic and allowing critical research to proceed when feasible during a challenging crisis. We are immensely grateful for the invaluable help, support, and assistance of the medical staff in facilitating study enrollment and interventions in the neurocritical unit in the middle of pandemic-related surges. The abstract for this publication has been submitted to the NeuroCriticalCare Society and the European Society of Neurosonology and Cerebral hemodynamics that are currently under review. Later part of this study was funded by a Pilot grant awarded by Neuroscience Clinical Trials and Innovations Center, Wake Forest School of Medicine.

Aarti Sarwal's institution has received compensation for research support for her role as site investigator for conducting multicenter clinical trial from Bard, Biogen, Novartis, and CVR Global, Inc. In addition, they have received compensation from LungPacer, Inc and NIH/NIA R01 AG066910-01 (Brinkley/Shaltout) for her role as a consultant for ultrasound image analysis in clinical research trials. She has received honorarium, free meeting registration, and/or reimbursement of travel expenses for role as speaker at continuing medical education activities conducted by Society of Critical Care Medicine, Neurocritical Society, Indian Society of Critical Care Medicine, Indian Academy of Neurology, American Institute of Ultrasound in Medicine, Intensive Care Society, American College of Chest Physicians, American Thoracic Society, and American Association of Physical Therapists. The remaining authors declare no conflict of interest.

ORCID

Sahil Kapoor https://orcid.org/0000-0003-3553-382X
Andrew Asimos https://orcid.org/0000-0002-6697-3724

REFERENCES

1. Patel Y, D'Agostino R Jr, Brown P, et al. Exploratory study to assess feasibility of intracranial hemorrhage detection by point of care cranial ultrasound. Under Review Neurocritic Care 2022.
2. Sarwal A, Elder N. Point-of-care cranial ultrasound in a hemicraniectomy patient. Clin Pract Cases Emerg Med Nov 2018;2:375–7.
3. Alonso-Canovas A, Lopez-Sendon Moreno JL, Buisan J, et al. Does normal substantia nigra echogenicity make a difference in Parkinson's disease diagnosis? A real clinical practice follow-up study. J Neurol 2018;265:2363–9.
4. Bor-Seng-Shu E, Pedroso JL, Felicio AC, et al. Substantia nigra echogenicity and imaging of striatal dopamine transporters in Parkinson's disease: a cross-sectional study. Parkinsonism and Relat Disord 2014;20:477–81.
5. Iranzo A, Lomeña F, Stockner H, et al. Decreased striatal dopamine transporter uptake and substantia nigra hyperechogenicity as risk markers of synucleinopathy in patients with idiopathic rapid-eye-movement sleep behaviour disorder: a prospective study. Lancet Neurol 2010;9:1070–7.
6. Prell T, Schenk A, Witte OW, Grosskreutz J, Günther A. Transcranial brainstem sonography as a diagnostic tool for amyotrophic lateral sclerosis. Amyotroph Lateral Scler Frontotemporal Degener 2014;15:244–9.
7. Walter U, Dressler D, Wolters A, Probst T, Grossmann A, Benecke R. Sonographic discrimination of corticobasal degeneration vs progressive supranuclear palsy. Neurology 2004;63:504–9.
8. Bártová P, Kraft O, Bernátek J-R, et al. Transcranial sonography and (123)I-FP-CIT single photon emission computed tomography in movement disorders. Ultrasound Med Biol 2014;40:2365–71.
9. Budisic M, Bosnjak J, Lovrencic-Huzjan A, Mikula I, Bedek D, Demarin V. Pineal gland cyst evaluated by transcranial sonography. Eur J Neurol 2008;15:229-33.
10. Budisić M, Bosnjak J, Lovrencić-Huzjan A, et al. Transcranial sonography in the evaluation of pineal lesions: two-year follow up study. Acta Clin Croat 2008;47:205–10.
11. Doepp F, Plotkin M, Siegel L, et al. Brain parenchyma sonography and 123I-FP-CIT SPECT in Parkinson's disease and essential tremor. Mov Disord 2008;23:405–10.
12. Gaenslen A, Unmuth B, Godau J, et al. The specificity and sensitivity of transcranial ultrasound in the differential diagnosis of Parkinson's disease: a prospective blinded study. Lancet Neurol 2008;7:417–24.
13. Hagenah JM, König IR, Becker B, et al. Substantia nigra hyperechogenicity correlates with clinical status and number of Parkin mutated alleles. J Neurol 2007;254:1407–13.
14. Hellwig S, Reinhard M, Amtage F, et al. Transcranial sonography and [18F]fluorodeoxyglucose positron emission tomography for the differential diagnosis of parkinsonism: a head-to-head comparison. Eur J Neurol 2014;21:860–6.
15. Li D-H, Zhang L-Y, Hu Y-Y, et al. Transcranial sonography of the substantia nigra and its correlation with DAT-SPECT in the diagnosis of Parkinson's disease. Parkinsonism Relat Disord 2015;21:923–8.
16. Mašková J, Školoudík D, Burgetová A, et al. Comparison of transcranial sonography-magnetic resonance fusion imaging in Wilson's and early-onset Parkinson's diseases. Parkinsonism Relat Disord 2016;28:87–93.
17. Postert T, Lack B, Kuhn W, et al. Basal ganglia alterations and brain atrophy in Huntington's disease depicted by transcranial real time sonography. J Neurol Neurosurg Psychiatry 1999;67:457–62.
18. Mäurer M, Shambal S, Berg D, et al. Differentiation between intracerebral hemorrhage and ischemic stroke by transcranial color-coded duplex-sonography. Stroke 1998;29:2563–7.
19. Tribl GG, Bor-Seng-Shu E, Trindade MC, Lucato LT, Teixeira MJ, Barbosa ER. Wilson's disease presenting as rapid eye movement sleep behavior disorder: a possible window to early treatment. Arq Neuropsiquiatr 2014:72:653–8
20. Berg D, Supprian T, Hofmann E, et al. Depression in Parkinson's disease: brainstem midline alteration on transcranial sonography and magnetic resonance imaging. J Neurol 1999;246:1186–93.
21. Walter U, Krolikowski K, Tarnacka B, Benecke R, Czlonkowska A, Dressler D. Sonographic detection of basal ganglia lesions in asymptomatic and symptomatic Wilson disease. Neurology 2005;64:1726–32.
22. Brüggemann N, Hagenah J, Reetz K, et al. Recessively inherited parkinsonism: effect of ATP13A2 mutations on the clinical and neuroimaging phenotype. Arch Neurol 2010;67:1357–63.
23. Woydt M, Greiner K, Perez J, Becker G, Krone A, Roosen K. Transcranial duplex-sonography in intracranial hemorrhage. Evaluation of transcranial duplex-sonography in the diagnosis of spontaneous and traumatic intracranial hemorrhage. Zentralbl Neurochir 1996;57:129–35.

24. Rossler L, Ludwig-Seibold C, Thiels Ch, Schaper J. Aicardi-Goutières syndrome with emphasis on sonographic features in infancy. Pediatr Radiol 2012;42:932–40.
25. Becker G, Winkler J, Hofmann E, Bogdahn U. Differentiation between ischemic and hemorrhagic stroke by transcranial color-coded real-time sonography. J Neuroimaging 1993;3:41–7.
26. Camps-Renom P, Méndez J, Granell E, et al. Transcranial duplex sonography predicts outcome following an intracerebral hemorrhage. AJNR Am J Neuroradiol 2017;38:1543–9.
27. Becker G, Greiner K, Kaune B, et al. Diagnosis and monitoring of subarachnoid hemorrhage by transcranial color-coded real-time sonography. Neurosurgery 1991;28:814–20.
28. Weise D, Lorenz R, Schliesser M, Schirbel A, Reiners K, Classen J. Substantia nigra echogenicity: a structural correlate of functional impairment of the dopaminergic striatal projection in Parkinson's disease. Mov Disord 2009;2:1669–75.
29. Scherfler C, Esterhammer R, Nocker M, et al. Correlation of dopaminergic terminal dysfunction and microstructural abnormalities of the basal ganglia and the olfactory tract in Parkinson's disease. Brain 2013;136:3028–37.
30. Schweitzer KJ, Hilker R., Walter U, Burghaus L, Berg D. Substantia nigra hyperechogenicity as a marker of predisposition and slower progression in Parkinson's disease. Mov Disord 2006;2:94–8.
31. Sprenger FS, Wurster I, Seppi K, et al. Substantia nigra hyperechogenicity and Parkinson's disease risk in patients with essential tremor. Mov Disord 2016;31:579–83.
32. Vlaar AM, De Nijs T, Van Kroonenburgh MJ, et al. The predictive value of transcranial duplex sonography for the clinical diagnosis in undiagnosed parkinsonian syndromes: comparison with SPECT scans. BMC Neurol 2008;8:42.
33. Kivi A, Trottenberg T, Kupsch A, Plotkin M, Felix R, Niehaus L. Levodopa-responsive posttraumatic parkinsonism is not associated with changes of echogenicity of the substantia nigra. Mov Disord 2005;20:258–60.
34. Pedroso JL, Bor-Seng-Shu E, Braga-Neto P, et al. Neurophysiological studies and non-motor symptoms prior to ataxia in a patient with machado-joseph disease: trying to understand the natural history of brain degeneration. Cerebellum 2014;13:447–51.
35. Ebentheuer J, Canelo M, Trautmann E, Trenkwalder C. Substantia nigra echogenicity in progressive supranuclear palsy. Mov Disord. 30 2010;25:773–7.
36. Seidel G, Kaps M, Dorndorf W. Transcranial color-coded duplex sonography of intracerebral hematomas in adults. Stroke 1993;24:1519–27.
37. Lindner A, Gahn G, Becker G. Transcranial duplex sonography of hyperacute intracerebral hemorrhages. J Neuroimaging 1997;7:199–200.
38. Masaeli M, Chahardoli M, Azizi S, et al. Point of care ultrasound in detection of brain hemorrhage and skull fracture following pediatric head trauma; a diagnostic accuracy study. Arch Acad Emerg Med 2019;7:e53.
39. Matsumoto N, Kimura K, Iguchi Y, Aoki J. Evaluation of cerebral hemorrhage volume using transcranial color-coded duplex sonography. J Neuroimaging 2011;21:355–8.
40. Mäurer M, Shambal S, Berg D, et al. Differentiation between intracerebral hemorrhage and ischemic stroke by transcranial color-coded duplex-sonography. Stroke 1998;29:2563–7.
41. Niesen W-D, Schläger A, Reinhard M, Fuhrer H. Transcranial sonography to differentiate primary intracerebral hemorrhage from cerebral infarction with hemorrhagic transformation. J Neuroimaging 2018;28:370–3.
42. Niesen W-D, Schlaeger A, Bardutzky J, Fuhrer H. Correct outcome prognostication via sonographic volumetry in supratentorial intracerebral hemorrhage. Front Neurol 2019;10:492
43. Ovesen C, Christensen AF, Krieger DW, Rosenbaum S, Havsteen I, Christensen H. Time course of early postadmission hematoma expansion in spontaneous intracerebral hemorrhage. Stroke 2014;45:994–9.
44. Wang H-S, Kuo M-F, Huang S-C, Chou M-L, Hung Po-C, Lin K-L. Transcranial ultrasound diagnosis of intracranial lesions in children with headaches. Pediatr Neurol 2002;26:43–6.
45. Kern R, Kablau M, Sallustio F, et al. Improved detection of intracerebral hemorrhage with transcranial ultrasound perfusion imaging. Cerebrovasc Dis 2008;26:277–83.
46. Kukulska-Pawluczuk B, Książkiewicz B, Nowaczewska M. Imaging of spontaneous intracerebral hemorrhages by means of transcranial color-coded sonography. Eur J Radiol 2012;81:1253–8.
47. Seidel GN, Md HCR, Albers T, Meyer-Wiethe K. Transcranial sonographic monitoring of hemorrhagic transformation in patients with acute middle cerebral artery infarction. Journal of Neuroimaging 2005;15:326–30.
48. Seidel G, Canguìr H, Albers T, Burgemeister A, Meyer-Wiethe K. Sonographic evaluation of hemorrhagic transformation and arterial recanalization in acute hemispheric ischemic stroke. Stroke 2009;40:119–23.
49. Niesen W-D, Rosenkranz M, Weiller C. Bedsided transcranial sonographic monitoring for expansion and progression of subdural hematoma compared to computed tomography. Front Neurol 2018;9:374
50. Niesen W-D, Burkhardt D, Hoeltje J, Rosenkranz M, Weiller C, Sliwka U. Transcranial grey-scale sonography of subdural haematoma in adults. Ultraschall Med 2006;27:251–5.
51. Lacerda FH, Rahhal H, Soares LJ, Ureña FDRM, Park M. Intracranial epidural hematoma follow-up using bidimensional ultrasound. Rev Bras Ter Intensiva 2017;29:259–60.
52. Becker G, Krone A, Koulis D, et al. Reliability of transcranial colour-coded real-time sonography in assessment of brain tumours: correlation of ultrasound, computed tomography and biopsy findings. Neuroradiology 1994;36:585–90.
53. Becker G, Krone A, Schmitt K, et al. Preoperative and postoperative follow-up in high-grade gliomas: comparison of transcranial color-coded real-time sonography and computed tomography findings. Ultrasound Med Biol 1995;21:1123–35.
54. Becker G, Hofmann E, Woydt M, et al. Postoperative neuroimaging of high-grade gliomas: comparison of transcranial sonography, magnetic resonance imaging, and computed tomography. Neurosurgery 1999;44:469–77.
55. Meyer K, Seidel G, Knopp U. Transcranial sonography of brain tumors in the adult: an in vitro and in vivo study. J Neuroimaging 2001;11:287–92.
56. Phillips SB, Gates M, Krishnamurthy S. Strategic placement of bedside ventriculostomies using ultrasound image guidance: report of three cases. Neurocrit Care 2012;17:255–9.

SUPPORTING INFORMATION

Additional supporting information can be found online in the Supporting Information section at the end of this article.

How to cite this article: Kapoor S, Offnick A, Allen B, Brown PA, Sachs JR, Gurcan MN, et al. Brain topography on adult ultrasound images: Techniques, interpretation, and image library. J Neuroimaging. 2022;32:1013–1026. https://doi.org/10.1111/jon.13031